EurJIC European Journal of Inorganic Chemistry

ChemPubSoc Europe

FULL PAPER

DOI:10.1002/ejic.201201507

Homoleptic Bis(aryl)acenaphthenequinonediimine–Cu^{I} Complexes – Synthesis and Characterization of a Family of Compounds with Improved Light-Gathering Characteristics

Panagiotis Papanikolaou,*[a,b] Pericles D. Akrivos,[a] Agnieszka Czapik,[c] Barbara Wicher,[c] Maria Gdaniec,*[c] and Nikolai Tkachenko*[b]

Keywords: Copper / N ligands / Electronic structure / Structure elucidation

A group of bis(aryl)acenaphthenequinonediimine (Ar-BIAN) ligands were synthesized through a modified procedure, which bypasses the need for absolutely dry conditions during the initial template synthesis. The molecular and electronic structure of the corresponding homoleptic $[Cu(Ar\text{-}BIAN)_2]$-BF_4 complexes were probed by means of a variety of spectroscopic methods. In accord with solution ^{13}C NMR spectra, X-ray crystallography reveals D_2 or approximate D_2 symmetry for the $[Cu(p\text{-}Cl\text{-}BIAN)_2]^+$ and $[Cu(p\text{-}Me\text{-}BIAN)_2]^+$ cations and noncrystallographic C_2 symmetry for the $[Cu(o\text{-}Ph\text{-}BIAN)_2]^+$ cation. The structures of the *p*-Cl-, *p*-Me, and *o*-Ph-BIAN complexes agree with the presence of ligands in their neutral form according to the lengths of the relevant C–C and C=N bonds of the organic skeleton. The concerted stereo–electronic effects of the substituents on the aryl rings affect the electron donor/acceptor capacities of the ligands and the structures of the complexes, as the study of the visible absorption spectra of the complexes indicates. The spectra of the complexes are dominated by intense and broad metal-to-ligand charge transfer (MLCT) bands that enter the near-infrared (NIR) region. Additionally, electrochemical studies undertaken reveal several successive electron capture and release processes, which further manifest the redox versatility of the ligands.

Introduction

The emerging need for renewable energy sources, in particular solar radiation, has turned scientific interest towards the discovery and manipulation of the behavior of new photoactive materials[1] that can capture, store, and redirect or re-release energy more efficiently. Although the main concern has been devoted to second and third row transition-metal complexes with bi- or tridentate polypyridyl ligands,[2] copper(I) compounds bearing mainly 2,9-disubstituted phenanthrolines emerged recently as an alternative with many potential applications in lighting technologies.[3] These copper(I) compounds do not have the high cost and environmentally hazardous nature of the former compounds.

Despite the advantages of Cu^{I} complexes, one of the main goals still to achieve is the synthesis of materials that absorb in the red and near-infrared (NIR) part of the spectrum. In 1999, Miller and Karpishin reported the synthesis of a Cu^{I} black absorber that bears two phenylethynyl-disubstituted phenanthroline ligands.[4] The aim of this work was to investigate the possibility of redshifting the energy of the metal-to-ligand charge transfer (MLCT) absorption by lowering the energy of the π*-acceptor orbitals of the diimine through enhancement of the electronic delocalization and to study its impact on the photophysics and photochemistry of the system. The authors concluded that to expand the absorption of the Cu^{I}–bisdiimine systems a substantial distortion of the molecule from the ideal D_{2d} symmetry is required. This results in poor photophysical behavior further underpinned according to the energy gap law by an extended delocalization that reduces the energy gap between the ground state and the excited MLCT state.

In this paper, we report the synthesis, characterization, structure, and optical and redox properties of a group of Cu^{I} NIR absorbers with a series of exocyclic diimines as ligands (Figure 1). The bis(aryl)acenaphthenequinonedi-

[a] Dept. of Chemistry, Aristotle University of Thessaloniki
P.O.B. 135, 54124 Thessaloniki, Greece
Fax: +30-2310-997738
E-mail: panpapan@chem.auth.gr
[b] Tampere University of Technology, Faculty of Science and Environmental Engineering, Department of Chemistry and Bioengineering,
33101 Tampere, Finland
E-mail: nikolai.tkachenko@tut.fi
Homepage: http://kemia.me.tut.fi/nick
[c] Faculty of Chemistry, Adam Mickiewicz University,
ul. Grunwaldzka 6, 60-780 Poznan, Poland
E-mail: magdan@amu.edu.pl
Homepage: http://www.chemia.amu.edu.pl/main/staff/Gdaniec.htm

Supporting information for this article is available on the WWW under http://dx.doi.org/10.1002/ejic.201201507.

© 2013 Wiley-VCH Verlag GmbH & Co. KGaA, Weinheim

imine (Ar-BIAN) series was selected for this purpose as the enhanced delocalization of the acenaphthenequinone central skeleton can reduce the energy of the MLCT absorption compared to those of the ordinary diimines reported to date. Although these ligands have been used in many studies for catalytic purposes,[5] some publications with heavier metals[6] raised our interest in the photophysics of compounds bearing these redox active molecules. Additionally, these latter systems have been proposed as potent components in bulk heterojunction photovoltaic devices.[7] The electronic behavior of the Ar-BIAN molecules appears to be rich as they can act as efficient "electron sponges" and store up to four electrons, [8] which results in the respective anionic forms,[9] and recently they have been shown to form stable radicals following coordination to several metal centers.[10] Our studies indicate that although the Cu^{I} center adopts an almost tetrahedral coordination in the solid state, its geometry in solution is flattened as is revealed by the rise of a low-energy shoulder accompanying the MLCT absorption maximum. The bathochromic shift imposed by the electronic system of the ligands results in an enhanced absorption of the complexes that extends into the NIR region of the spectrum.

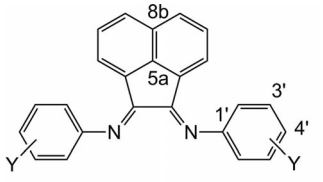

Y = *p*-MeO (**1**), *p*-Me (**2**), *p*-Cl (**3**), *o*-Ph (**4**), *m*-Cl (**5**), *m*-CF_3 (**6**)

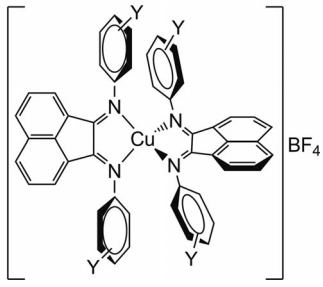

Figure 1. Schematic representation of the Ar-BIAN ligands and the corresponding homoleptic Cu^{I} tetrafluoroborate complexes studied. The position of the substituent on the phenyl rings is relative to the imine nitrogen atoms.

Results and Discussion

Synthesis

Except for *m*-Cl-BIAN, the ligands have been reported previously and their characterization was confirmed by comparison with the published data.[7b,11–13] The *m*-Cl-BIAN ligand was characterized in an analogous manner as the other members of this group, in particular the 3,5-dichloro-substituted one.[11] The Cu^{I} complexes were isolated as air stable almost black powders with quite interesting optical and electrochemical behavior as will be discussed below. The color of the free ligands in dichloromethane varies from yellow to deep red. The dichloromethane solutions of the complexes bearing the *p*-Cl, *o*-Ph, *m*-Cl, and *m*-CF_3 substituents are deep purple, whereas those with *p*-MeO and *p*-Me substitution are dark green and dark blue, respectively.

A point to be discussed is the nature of the isolated complexes. The ligands used in this study are known for their tendency to stabilize radical species after their reactions with the main group metals[10i,10j,10k] and first row transition elements,[10l] which results in noninnocent behavior.[14,10l] Therefore, the question arises about the oxidation state of both the metal center and the ligands. Together with EPR spectroscopy, the safest way to assign the electronic structure of redox-active molecules is crystallographic analysis, as significant differences are expected in bond lengths with different numbers of accommodated electrons.[10l,15] The X-ray results verify that the stoichiometry of the complexes agrees with the existence of a Cu^{I} center and that the coordinated BIAN ligands are structurally identical to the neutral Ar-BIAN molecules within experimental error.[12,13,16–18] Additionally, the lineshape of the NMR spectra for the complexes is another strong sign of the lack of any paramagnetic behavior, which would result from the formation of radical metal or ligand species. Therefore, we think it is safe to assign the metal center as Cu^{I} and the ligands in their neutral closed-shell structure.

Vibrational Spectroscopy

The IR spectra of the free ligands are characterized by the presence of a weak band in the region 3045–3060 cm^{-1}, which is assigned to the stretching vibration of the =C–H bonds present in all of them, whereas the C–H bond vibrations for the *p*-MeO-BIAN and the *p*-Me-BIAN ligands are observed as weak peaks at 2948 and 2914 cm^{-1}, respectively. All of the spectra demonstrate a set of two strong absorptions in the region 1669–1617 cm^{-1}, which are assigned to the stretching vibration of the imine bonds although such an assignment cannot be unambiguous as the stretching frequencies of the naphthalene C=C bonds also appear in the same region.[19] The absence of any absorption above 1700 cm^{-1} confirms the purity of the compounds and excludes the presence of the 1:1 condensation byproduct of the diketone and the substituted anilines.[20,21] The imine bond absorption of the complexes appears as one peak in the region 1644–1634 cm^{-1}. The shift to lower wavenumbers on coordination is due to the weakening of the C=N bond, and the appearance of a single peak is indicative of the coordination of the diimines in a chelating manner.[17] The magnitude of the observed shifts further supports the hypothesis that the ligands are present in the complexes in their neutral oxidation state,[22,23] as in their corresponding radical or anionic forms the C–N bonds would be expected to reveal considerably larger shifts.[10k] Ad-

 © 2013 Wiley-VCH Verlag GmbH & Co. KGaA, Weinheim

ditionally, the characteristic bands of the methyl group stretches are present in the typical positions of the methyl- and methoxy-substituted BIAN ligands, and their positions shift slightly upon coordination. In the spectra of the copper complexes, there is generally a strong band with a broad maximum at 1050–1060 cm^{-1}, which is indicative of the presence of tetrafluoroborate counteranions, however in some cases this band appears to be split. This is probably due to intra- or intermolecular interactions of the anion, which result in breakdown of the local T_d symmetry.[24]

Solution NMR Spectroscopy

Ragaini et al. reported the solution behavior of Ar-BIAN ligands.[25] These molecules can exist in two different isomers denoted as *anti–anti* and *syn–anti*, which refer to the imine bonds (Scheme 1). Although asymmetric Ar-BIAN molecules do appear in both forms in solution, symmetric ones seem to occur only as the *anti–anti* isomer. From the number of peaks in the ^{13}C NMR spectra of the ligands under study, this is also confirmed for ligands **1**, **2**, **3** and **5**, whereas **4** and **6** are characterized by the existence of additional signals. For these two latter cases, the peaks could be assigned either to the existence of the *syn–anti* molecule in solution as a minor isomer or to the inequivalence of the ligand carbon atoms owing to sterically hindered rotation of the phenyl pendant rings. The presence of two isomers in solution does not alter the reactivity of the Ar-BIAN ligands.[25,26] Although the ^{13}C-NMR spectrum of [Cu(**4**)$_2$]BF_4 is characterized by an excessive number of signals as will be discussed further below, the spectrum of [Cu(**6**)$_2$]BF_4 reveals the expected number of signals, which indicates that the extra signals in **6** belong to the *syn–anti* isomer and that it transforms to the *anti–anti* one after complexation with the metal center.

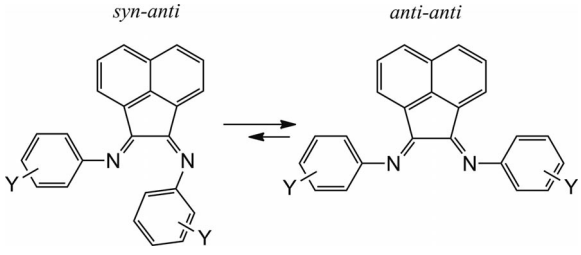

Scheme 1.

In the NMR spectra recorded in $CDCl_3$, the typical resonances expected for the proton and carbon atoms of the Ar-BIAN ligands are observed. In particular, and as expected, the methyl proton and carbon resonances of the 4-Me and 4-MeO ligands do not shift upon coordination. Very small shifts are observed for the resonances of the characteristic imino carbon atoms and the aryl group directly attached to the nitrogen atom. In the ^{13}C spectra, a single line is observed for each chemically equivalent set of atoms, which indicates that equilibration occurs in solution and, therefore, steric crowding or π–π intra- or intermolecular interactions are not important in the determination of the overall structure of the compounds in solution. For **4** and **6**, the spectroscopic data listed in the experimental section, especially the ^1H NMR data, refer mainly to the major isomer although a clear separation was not possible. From the integration of proton signals, the ratio of the two isomers appears to be 5:1 for **4** and 20:1 for **6**.

In the solution ($CDCl_3$) NMR spectra of the complexes, the ^1H and ^{13}C resonances are observed in the typical regions, which suggests that they comprise neutral Ar-BIAN ligands coordinated to Cu^I centers. The spectra are dominated by the resonances of the aromatic rings, and their assignment was carried out in accordance with previously published results.

The ^{13}C NMR spectra are more informative of the coordination of the ligands. The relevant resonances of the imino carbon atom, the 5a and 8b carbon atoms of the acenaphthene backbone, and the carbon atom at the 1′-position of the aryl substituents along with the one bearing the substituent are reported in Table 1. The carbon atoms of the acenaphthene skeleton reveal a slight shift upon coordination, which is not uniform and is, therefore, ascribed to the aryl ring substituent rather than to the coordination itself. The value of the imino carbon resonance is very consistent throughout the ligand series and undergoes a lower

Table 1. ^{13}C NMR spectroscopic data for the most relevant carbon atoms of the ligands and the copper complexes studied (for numbering scheme see Figure 1). Chemical shifts are reported in ppm downfield from internal TMS standard. Primed numbers refer to the pendant aryl rings and Y to the carbon of the aryl ring substituent.

Compound	Imino	1′	5a	8b	3′, 4′	Y
1	161.8	157.1	145.1	141.9	129.1	55.7
[Cu(**1**)$_2$]BF_4	163.0	159.4	142.5	140.2	131.5	56.0
2	161.5	149.4	141.9	131.4	134.1	21.3
[Cu(**2**)$_2$]BF_4	163.8	145.1	142.9	131.5	138.0	21.5
3	161.9	150.2	142.1	130.1	131.5	–
[Cu(**3**)$_2$]BF_4	163.4	145.7	141.8	130.9	131.2	–
4	160.9	149.7	141.5	139.4	131.3	–
[Cu(**4**)$_2$]BF_4	164.2–165.6	144.3–145.1	141.8–142.4	137.4–138.2	[a]	–
5	161.9	152.9	142.2	131.5	135.3	–
[Cu(**5**)$_2$]BF_4	165.0	148.5	143.5	132.2	136.0	–
6	162.0	152.0	142.3	132.4	–	115.6
[Cu(**6**)$_2$]BF_4	165.2	147.6	143.5	132.8	–	116.8

[a] Several signals observed.

 © 2013 Wiley-VCH Verlag GmbH & Co. KGaA, Weinheim

field shift upon coordination. The same is also true for the carbon atoms of the aryl rings that bear the substituent, whereas an opposite trend is observed for the carbon atom attached to the imine site. In all cases, a single signal is observed for each carbon atom with the exception of the *o*-phenyl-substituted Ar-BIAN, for which quartets are observed within small margins in typical region of 120–130 ppm for the more downfield resonances. This is attributed to the severely crowded nature of the ligand around the diimine coordination site, which prevents the typical equilibration through fast rotation about the single bonds that connect the aryl rings to each other and to the central backbone of the ligand. However, the average shift of each group of lines relative to the one observed for the free ligand follows the observations made for the other compounds.

Electrochemical Studies

The redox behavior of the Ar-BIAN ligands and their Cu^{I} homoleptic complexes in dichloromethane containing 0.1 M tetrabutylammonium tetrafluoroborate as supporting electrolyte was investigated by differential pulse voltammetry (DPV). The obtained redox potentials (V vs. Ag wire) have some common characteristics presented below. For the ligands, there are two reduction processes in the regions –1.10 to –1.25 V (–1.78 to –1.93 V vs. Fc^{+}/Fc) and –1.69 to –1.87 V (–2.37 to –2.55 V vs. Fc^{+}/Fc). There are also two distinct oxidation peaks in the regions +1.45 to +1.65 (0.77 to 0.97 V vs. Fc^{+}/Fc) and +1.75 to +1.98 V (1.07 to 1.30 V vs. Fc^{+}/Fc) with the notable exception of **1**, for which the two oxidation peaks are observed at +1.20 and +1.64 V (0.52 and 0.96 V vs. Fc^{+}/Fc respectively).

The voltamogramms of the complexes reveal a more complicated pattern with up to four reduction and oxidation processes. Generally, the reduction peaks are reversible and the oxidation ones are not. The first peak observed close to +0.6 V (–0.08 V vs. Fc^{+}/Fc) may be attributed to metal-centered processes, however in view of the noninnocent character of the ligands, strong participation of the diiminic region or even formation of species with delocalized electron density cannot be overlooked. Oxidation at potentials of over + 1.0 V (0.32 V vs. Fc^{+}/Fc) are most probably related to ligand-based processes affected to a small extent by the presence of the metal core. Such phenomena could take place in a region of the ligand away from the Cu^{I} center such as the naphthyl part. In some cases, there are close lying and even overlapping peaks, which suggests successive one- and two-electron transfer processes or even the existence of chemical processes such as fragmentation of radical species coupled to the electron transfers.[27] Finally, reductive signals at ca. –0.6 V (–1.28 V vs. Fc^{+}/Fc) could correspond to the formation of Cu^{0} species or reduction of the diiminic region of the ligands stabilized by the presence of the metal center, and those at more negative potentials could be related to anionic species with the negative charge located on the organic skeleton of the molecules as is well documented for the series of Ar-BIAN ligands. Under the same experimental conditions the ferrocene/ferrocenyl oxidation potential was observed at +0.68 V.

Visible Spectroscopy

The spectra of the ligands in dichloromethane show intense absorptions in the UV region and a broad chromophoric band that extends to ca. 500 nm (Figure 2). The UV absorptions are π–π* in nature and display variations attributed to the substituents on the pendant phenyl rings. The broad band in the visible part of the spectra could be assigned to n–π* transitions potentially involving a partial charge transfer from the imine region or the phenyl rings (intraligand π–π* charge transfer) to the naphthyl backbone of the molecules. The intensity differences of this band in various solvents do not reveal any apparent regularity and are ascribed to conformational changes induced by solvent–solute interactions. Such interactions should affect the electronic communication between the pendant phenyl rings and the acenaphthenequinone main skeleton, which supports further the proposed partial CT character. However, the solvatochromic shifts observed are very small.

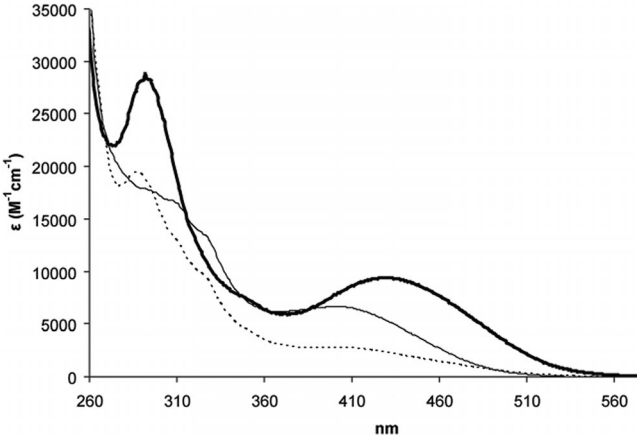

Figure 2. UV/Vis spectra of representative Ar-BIAN ligands in dichloromethane solution. The curves correspond to **1**- (bold), **3**- (thin), and **4**-substituted (dashed) Ar-BIAN ligands.

Methoxy and chloro substituents at the *para* position of the phenyl rings give rise to enhanced visible absorption, which indicates that their action through conjugation causes incremental changes in the electronic density of the lone pair of the iminic nitrogen atoms and a decrease in the energy of the n–π* transitions. *para*-Methyl substitution appears to operate through its negative hyperconjugation effect, which depletes electron density from the π system of the main skeleton. The ligands with *meta* substituents reveal spectra with intensity features intermediate to the aforementioned ones and severe changes in the shape of the spectra are not observed, which indicates that their influence on the electronic wavefunction of the main chromophore is not significant. Finally, the *ortho*-phenyl substituent leads to an absorption pattern similar to that of the *p*-

 © 2013 Wiley-VCH Verlag GmbH & Co. KGaA, Weinheim

MeO one in the ultraviolet region. The maximum of the chromophoric band matches better that of the *p*-MeO and *p*-Cl substituents and its intensity follows that of the Me substituent.

The absorption of the homoleptic Cu^I complexes (Figure 3) covers the whole monitoring window in the form of two broad bands. The first has a maximum at ca. 350 nm with molar extinction coefficients greater than 20000 $M^{-1} cm^{-1}$ and is assigned to ligand-centered transitions, although partial MLCT character cannot be excluded. This band appears redshifted relative to those of the respective free ligands owing to the presence of the positively charged metal center. The second band is relatively intense with maxima in the visible region between 580 and 610 nm and extends to the NIR part of the spectrum. The results of theoretical calculations and the apparent similarity of this part of the spectrum to the MLCT absorption pattern of Cu^I–bis(phenanthroline) and related bisdiimine systems allows us to assign it as a MLCT transition.[4,28–33] Such transitions are generally characterized by high molar extinction coefficients and when they are the low lying as is the case for Cu^I systems, they result in long lifetimes of the excited state and potential luminescence.[34] In analogy to the MLCT band in $[Cu(phen)_2]^+$ systems, this absorption is considered as an envelope of at least three distinct excitations referred to as Bands I, II, and III.[34,35] Band I, which is totally forbidden for an ideal D_{2d} symmetry, corresponds to the excitation to the lowest singlet MLCT state (S1) and appears as a shoulder at the low energy side of the main visible absorption. The main part of the envelope, Band II, is assigned to the excitation to the third singlet MLCT state (S3),[36] and an additional MLCT absorption (Band III) is located at ca. 520 nm, overlapped by Band II. The low-lying π* orbitals of the acenaphthene moiety promote a considerable redshift relative to the typical corresponding Cu^I–diimine MLCT bands. The enhanced intensity of these bands can be related to the transition dipole length of the given excitations. Owing to the extended delocalization of the diimine π system, the π* accepting orbitals are spread away from the Cu^I center, which leads to an increased charge displacement during the excitation. This in turn results in an increased transition dipole length and enhanced absorptivity.[29]

As is generally accepted, the intensities of the above three bands are related to the symmetry of the complexes in solution. The low energy shoulder (Band I) serves as a fingerprint for the flattening distortion of the ground state geometry away from the ideal D_{2d} one,[34,35,27c] which renders the corresponding transition more allowed. In an effort to quantify this and in view of the crystallographic data available for three of the complexes, we proceeded with the computation of the intensity ratio of Band I to Band II. The digitized spectra were treated with the Peakfit algorithm by using the second-derivative technique for locating maxima. When the simulation reached an R^2 value of 0.9999, the sum of the individual Gaussian bands located within the low energy shoulder and the main part of the MLCT envelope and their intensity ratio were calculated. The results

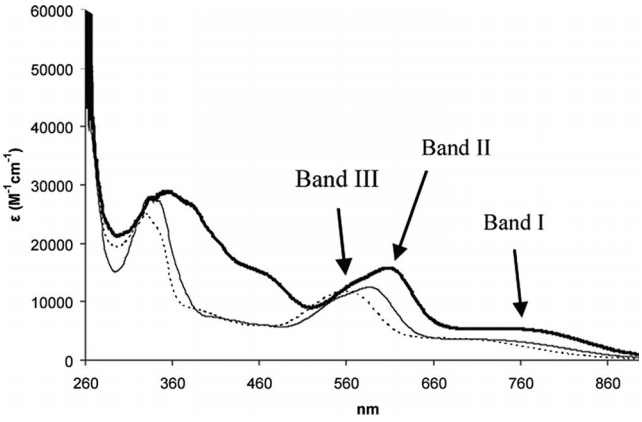

Figure 3. UV/Vis spectra of representative $[Cu(Ar\text{-}BIAN)_2]BF_4$ complexes in dichloromethane. Curves correspond to $[Cu(\mathbf{1})_2]BF_4$ (bold), $[Cu(\mathbf{3})_2]BF_4$ (thin), and $[Cu(\mathbf{4})_2]BF_4$ (dashed). Bands I, II and III, which result in the overall visible absorption, are indicated for $[Cu(\mathbf{1})_2]BF_4$ by arrows.

are reported in Table 2. The above ratio varies between 0.57 and 1.11. Consequently, the least planar geometry in solution is ascribed to $[Cu(\mathbf{2})_2]BF_4$ and the most distorted to $[Cu(\mathbf{1})_2]BF_4$. The following series for the ground state distortion emerges $[Cu(\mathbf{2})_2]BF_4 < [Cu(\mathbf{5})_2]BF_4 \approx [Cu(\mathbf{3})_2]BF_4 < [Cu(\mathbf{6})_2]BF_4 < [Cu(\mathbf{4})_2]BF_4 < [Cu(\mathbf{1})_2]BF_4$ and correlates well with the experimentally observed geometries as can be seen further below. For $[Cu(\mathbf{2})_2]BF_4$, $[Cu(\mathbf{3})_2]BF_4$, and $[Cu(\mathbf{4})_2]BF_4$, the dihedral angles between the two chelate rings are 85.6, 80.09, and 75.80°, respectively.

Table 2. Band maxima related to the excitations for the compounds studied in dichloromethane. ε^{780} refers to the absorption of the complexes at the specific wavelength as an indication of their NIR absorptivity.

Compound	$\lambda^{vis}{}_{max}$ [nm]	$\varepsilon^{vis}{}_{\lambda max}$ [$M^{-1} cm^{-1}$]	ε^{780} [($M^{-1} cm^{-1}$]	Intensity ratio
1	429	9400	–	–
2	409	3000	–	–
3	400	6650	–	–
4	402	2800	–	–
5	386 (sh)	4500	–	–
6	383 (sh)	4150	–	–
$[Cu(\mathbf{1})_2]BF_4$	609	15800	5030	1.11
$[Cu(\mathbf{2})_2]BF_4$	596	13800	2680	0.57
$[Cu(\mathbf{3})_2]BF_4$	587	12500	2730	0.66
$[Cu(\mathbf{4})_2]BF_4$	561	11750	1840	0.85
$[Cu(\mathbf{5})_2]BF_4$	579	10850	2270	0.64
$[Cu(\mathbf{6})_2]BF_4$	580	19750	1770	0.78

In the investigation of the solvatochromic shift of the MLCT absorption, it was observed that dissociation of the complexes takes place in coordinative solvents.[37] This means that there is a concentration-dependent substitution equilibrium between the diimines coordinated to the metal center and solvent molecules, which can be described by the reaction in Scheme 2, in which S corresponds to coordinative solvent molecules. Despite the exocyclic imine bonds of the Ar-BIAN ligands leading to an increased σ-donating ability compared to phenanthroline or bipyridine[20] and the

 © 2013 Wiley-VCH Verlag GmbH & Co. KGaA, Weinheim

enhanced π acidity of the main skeleton,[6,38] these complexes are not stable enough to prevent the formation of new species in a coordinative environment. Therefore, all the electronic spectroscopic studies were confined to dichloromethane solutions, in which two important observations were made. More precisely, the absorption spectra do not reveal the characteristic absorptions of the monoanionic Ar-BIAN radicals in the region 480–550 nm, which further supports that the diimines in these coordination compounds are in the typical neutral form.[10k] Additionally, luminescence studies carried out in optically diluted and carefully deaerated solutions produced no emission in the visible part of the spectrum after excitation of the MLCT band as has been previously observed for analogous systems.[39] This observation may be assigned to the energy gap law and to the lack of steric hindrance close to the metal center, which could prevent structural deformations in the excited state of the complexes.

$$[Cu(Ar\text{-}BIAN)_2]BF_4 \overset{S}{\rightleftharpoons} [Cu(Ar\text{-}BIAN)S_2]BF_4 + [Cu(S)_4]BF_4$$

Scheme 2.

X-ray Crystal Structures

As already mentioned, the safest way to assign the electronic structure of a redox-active organic molecule is to perform crystallographic studies. Our X-ray crystallography results reveal that the stoichiometry of the complexes agrees with the existence of a Cu^I center and that both of the coordinated Ar-BIAN molecules are structurally identical within experimental error and have bond lengths that match those of the neutral Ar-BIAN molecules.[12,13,17,18] The C–N and C–C bond lengths within the chelate rings fall within small margins around 1.28 and 1.50 Å, respectively, which are representative of the corresponding double and single bonds. For anionic ligands, the above values are ca. 1.35 and 1.45 Å, and for dianionic ligands, mainly observed for s- and p-block metal complexes, values of ca. 1.40 Å for both bonds have been recorded.[40]

The complex $[Cu(\mathbf{3})_2]BF_4$ (Figure 4, bottom) crystallizes in the orthorhombic system, space group *Ccca*, and both the coordination cation and the anion occupy special positions with 222 site symmetry. Its crystal structure is similar to that of the mesityl analogue [Cu(*o*,*o*′,*p*-CH_3-BIAN)]-BF_4·pentane.[39] However, the crystal structure of $[Cu(\mathbf{3})_2]BF_4$ was determined for the solvent-free form, which contained isolated voids of 83 $Å^3$ that form ca. 11% of the unit cell volume (Figure 5b).

The coordination environment of the Cu^I atom is strongly distorted tetrahedral, and because of the D_2 crystallographic symmetry of the coordination cation, all Cu–N bond lengths of 2.059(2) Å are equivalent. The imine C=N bonds are also equivalent and their length of 1.274(4) Å confirms the sp^2 character of the atoms involved. The BIAN bite angle is 81.90(12)°. The pendant aromatic rings adopt an almost perpendicular orientation relative to the

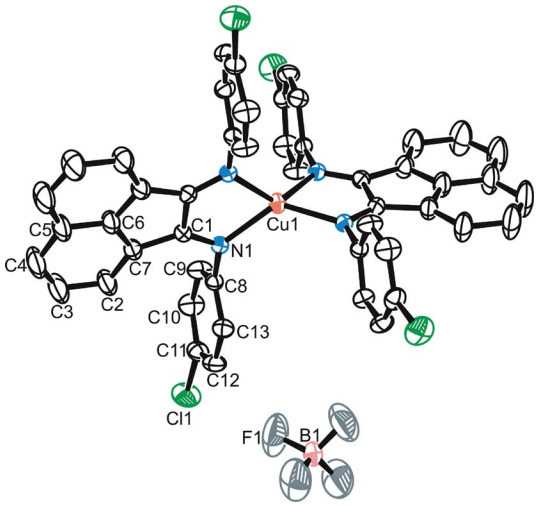

Figure 4. X-ray structures of $[Cu(\mathbf{2})_2]BF_4$·CH_2Cl_2 (top) and $[Cu(\mathbf{3})_2]BF_4$ (bottom). H atoms omitted for clarity. Only the asymmetric unit is labeled in each case. Solvent CH_2Cl_2 molecules exhibit disorder. Displacement ellipsoids are shown at the 30% probability level.

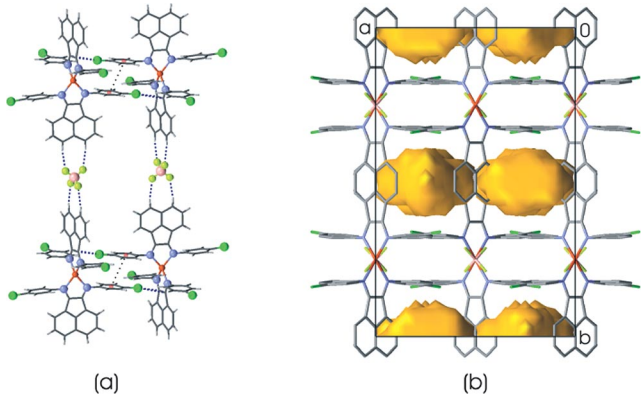

Figure 5. Crystal packing of $[Cu(\mathbf{3})_2]BF_4$. (a) Intermolecular interactions lead to the formation of a porous 3D framework and (b) twofold-interpenetrated 3D frameworks leave isolated empty voids of 83 $Å^3$ (H atoms are omitted for clarity).

acenaphthene plane, and the relevant dihedral angle is 88.6(1)°; the two chelate-ring planes are also almost perpendicular [dihedral angle 80.9(1)°]. This latter dihedral angle is similar to those found in the four symmetry-independent cations in $[Cu(p\text{-}i\text{Pr-BIAN})_2]BF_4$[41] (>80°) and is ca. 20° larger than those found in other D_2 symmetric complexes [Cu(*o*,*o*′,*p*-Me-BIAN)$_2$]BF_4·pentane (62.2°) and [Cu(*o*-*i*Pr-BIAN)$_2$]BF_4[41] (55.3°).

The crystal packing of $[Cu(\mathbf{3})_2]BF_4$ is best described as consisting of (010) layers of the coordination cations assembled through π–π stacking interactions of *p*-chlorophenyl groups (centroid–centroid distance 3.93 Å) and C–Cl···π interactions with the π system of the α-diimine group (Cl1···Cg 3.227 Å, <C11–Cl1···Cg 163.2°; Cg is the center of the C1–C1 bond). The neighboring (010) layers are bridged by the BF_4^- anions involved in C–H···F interactions to the acenaphthene H4 atoms (H4···F12 40 Å, <C4–H4···F1 168°), which results in a 3D porous framework

 © 2013 Wiley-VCH Verlag GmbH & Co. KGaA, Weinheim

(Figure 5, a). The crystal consists of two such 3D frameworks, which are related by the translation vector 1/2, 1/2, 0 and mutually interpenetrate (Figure 5, b).

The related 4-methyl compound $[Cu(\mathbf{2})_2]BF_4 \cdot 1.5CH_2Cl_2$ crystallizes in the monoclinic system, space group *C*2/*c*, and the asymmetric unit consists of the coordination cation $[Cu(\mathbf{2})_2]^+$, the BF_4^- anion, one CH_2Cl_2 molecule in a general position, and one half of a CH_2Cl_2 molecule disordered around an inversion center (Figure 4, top). The coordination to the metal center is not exactly symmetrical, and the Cu–N distances are in the range 1.992(2)–2.038(4) Å (Table 3). All these distances are shorter than the Cu–N distance in $[Cu(\mathbf{3})_2]BF_4$. The sp^2 character of the C and N atoms in the chelate ring is confirmed by the imine C=N bond lengths of 1.281(6)–1.296(5) Å. The two bite angles of the Ar-BIAN ligands are similar and are larger than those in the *p*-chlorophenyl analogue (Table 3). Three of the four pendant tolyl groups are strongly twisted relative to the central diimine plane with dihedral angles in the range 59.5(2)–69.6(2)°. The acenaphthene ring systems are not coplanar with the fused chelate rings and, thus, the dihedral angle between the two chelate rings of 86.5(2)° is significantly different from the dihedral angle between the acenaphthene best planes of 81.7(2)°. The crystal packing of this compound (Figure 6) is dominated by π–π stacking interactions between acenaphthene groups, which results in chains of the coordination cations extending along [112] and [–11–2]. In turn, the BF_4^- anions form a few short C–H···F contacts with CH_2Cl_2 solvent molecules and with the benzene ring (H44···F3 2.26 Å, <C44–H44···F3 143°).

The *o*-phenyl derivative $[Cu(\mathbf{4})_2]BF_4 \cdot 3CHCl_3$ crystallizes in the triclinic $P\bar{1}$ space group, and the asymmetric unit consists of the coordination cation $[Cu(\mathbf{4})_2]^+$, the BF_4^- anion, and three $CHCl_3$ solvent molecules (Figure 7, top). As is evident from Table 3, the coordination geometry around the Cu^I center is distorted tetrahedral and does not show any unusual features. The dihedral angle between the two chelate rings is 75.8(2)°. However, in contrast with the previously described complexes, the coordination cation

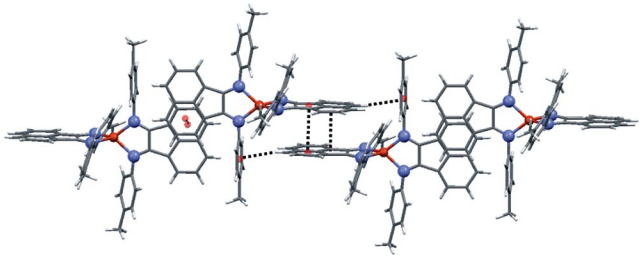

Figure 6. Crystal packing of $[Cu(\mathbf{2})_2]BF_4 \cdot 1.5CH_2Cl_2$. π–π stacking interactions between the acenaphthene groups and C–H···π interactions between the acenaphthene and tolyl groups lead to chains of coordination cations.

$[Cu(\mathbf{4})_2]^+$ has an approximate C_2 symmetry (Figure 7, bottom). This reduction in symmetry results from the conformation adopted by the *o*-Ph-BIAN ligand, in which both *ortho*-phenyl substituents point to the same site of the acenaphthene group. This structural change is probably caused by intramolecular C–H···π interactions between the biphenyl groups and not solely the bulkiness of the *ortho* substituent because in the recently reported *o*-*i*Pr-BIAN Cu^I complex the coordination cation had an approximate D_2 symmetry.[59] The attached benzene rings are twisted relative to the chelate rings and have twist angles in the range 67.6(3)–74.7(4)°. Moreover, all biphenyl groups in the cation show identical helicity as they are twisted around the central C–C bond by 42.2(4)–52.8(4)°. As in the crystals of $[Cu(\mathbf{2})_2]BF_4 \cdot 1.5CH_2Cl_2$, the crystal packing of this compound is dominated by π–π stacking interactions between acenaphthene groups (centroid–centroid distance 3.63–4.07 Å), which result in chains of coordination cations that extend along [011]. The BF_4 anions and chloroform molecules are accommodated in voids formed between the chains.

There are some marked differences between the structures reported here and those reported for similar compounds. Firstly, in the crystal structures reported here, which exhibit quite different patterns of intermolecular in-

Table 3. Selected bond lengths [Å] and angles [°] for the studied compounds.[a]

$[Cu(\mathbf{2})_2]BF_4 \cdot 1.5CH_2Cl_2$		$[Cu(\mathbf{3})_2]BF_4$		$[Cu(\mathbf{4})_2]BF_4 \cdot 3CHCl_3$	
Cu1–N1	2.012(3)	Cu1–N1	2.059(2)	Cu1–N1	2.0607(19)
Cu1–N2	2.033(4)			Cu1–N2	2.0216(18)
Cu1–N3	1.992(2)			Cu1–N3	2.0531(19)
Cu1–N4	2.038(4)			Cu1–N4	2.0353(18)
N1–C1	1.286(5)	N1–C1	1.274(4)	N1–C11	1.285(3)
N2–C2	1.294(5)			N1–C21	1.288(3)
C1–C2	1.504(6)	C1–C1^{i}	1.495(6)	C11–C21	1.497(3)
N3–C27	1.281(6)			N3–C12	1.286(3)
N4–C28	1.286(5)			N4–C22	1.283(3)
C27–C28	1.502(6)			C12–C22	1.503(3)
N3–Cu1–N1	124.10(14)	N1–Cu1–N1^{ii}	120.11(12)	N3–Cu1–N1	113.63(8)
N3–Cu1–N2	130.50(15)	N1–Cu1–N1^{iii}	129.74(12)	N3–Cu1–N2	133.04(8)
N1–Cu1–N2	83.12(15)	N1–Cu1–N1^{i}	81.90(12)	N1–Cu1–N2	82.39(8)
N3–Cu1–N4	82.80(15)			N3–Cu1–N4	82.56(7)
N1–Cu1–N4	121.24(15)			N1–Cu1–N4	129.82(8)
N2–Cu1–N4	120.28(14)			N2–Cu1–N4	121.95(7)

[a] Symmetry codes: (i) –*x*, *y*, –*z* + 1/2; (ii) –*x*, –*y* + 1/2, *z*; (iii) *x*, –*y* + 1/2, –*z* + 1/2.

© 2013 Wiley-VCH Verlag GmbH & Co. KGaA, Weinheim

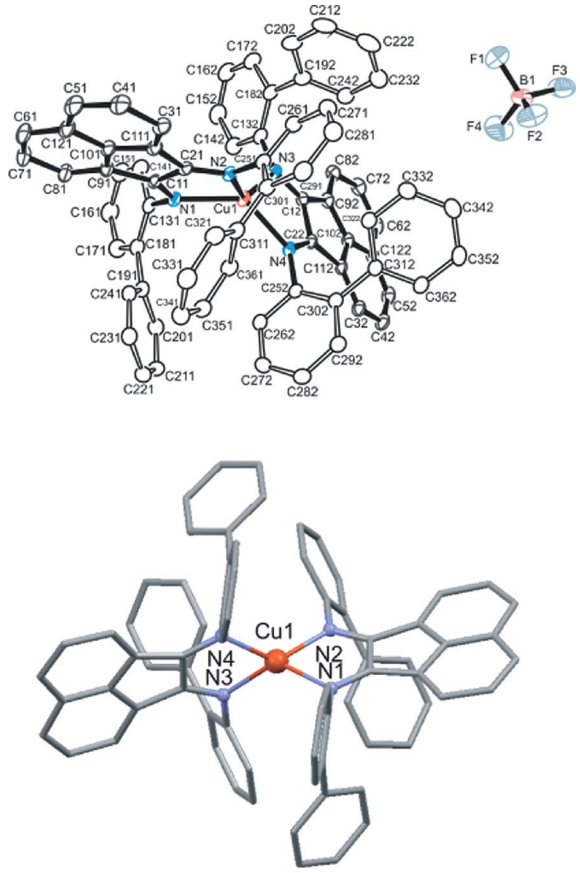

Figure 7. X-ray structure of $[Cu(\mathbf{4})_2]BF_4 \cdot 3CHCl_3$. ORTEP representation with atom labeling (top) and the noncrystallographic C_2 symmetry of the coordination cation with the twofold symmetry axis perpendicular to the figure plane and passing through Cu1 (bottom). H atoms and solvent $CHCl_3$ molecules omitted for clarity. Displacement ellipsoids are shown at the 30% probability level.

teractions, the dihedral angle between the two chelate rings (close to 90°) is ca. 20° larger than that for the earlier reported mesityl derivative.[39] Furthermore, for the mesityl and *o*,*o*-diisopropyl-substituted Ar-BIAN ligands, the Cu–N distances in the related $[Cu(Ar\text{-}BIAN)_2]^+$ and $[Cu(Ar\text{-}BIAN)(NCMe)_2]^+$ units are longer than the ones in our compounds, and the ligand bite angles are smaller and range in a small margin around 80°. Analogous differences are observed also relative to $[\{Cu(Ar\text{-}BIAN)\}_2(\mu\text{-}X)_2]$ dimers, for which there is asymmetry in the bonding of the Ar-BIAN ligand; the Cu–N bonds are longer, and the bite-angles are close to 80°.[18] The same observations hold also for a series of heteroleptic copper(I) complexes with BIAN-type ligands and phosphanes.[38]

Molecular Geometry Calculations

The geometry of the $[Cu(\mathbf{3})_2]^+$ cation was optimized in a dichloromethane medium by utilizing the polarizable continuum model (PCM).[42] A relevant view of the final structure is given in Figure 8, the atomic coordinates of the optimized structure are available in the Supporting Information, and the relevant geometrical parameters are given in Table 4.

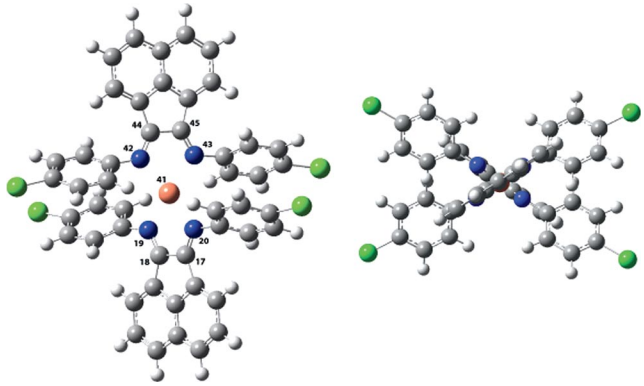

Figure 8. Different views and atom numbering of the optimized structure of $[Cu(\mathbf{3})_2]^+$. The twist of the pendant phenyl rings relative to the acenaphthene skeleton and the distortion from the ideal tetrahedral structure are in accordance with the experimental evidence.

Table 4. Relevant optimized bond lengths and angles for $[Cu(\mathbf{3})_2]^+$. A complete list of atomic parameters and numbering are provided in the Supporting Information.

Bond	Length [Å]	Bond	Angle [°]
Cu–N19	2.112	N19–Cu–N20	80.25
Cu–N20	2.108	N42–Cu–N43	80.25
Cu–N42	2.108	N19–Cu–N43	135.21
Cu–N43	2.112	N20–Cu–N42	136.61
C44–C45	1.516	–	–
C17–C18	1.516	–	–
C17–N19	1.292	–	–
C18–N20	1.292	–	–

A distortion towards a flattened geometry is revealed and, in view of the crystal structure of the compound, its geometry alteration upon dissolution is opposite to the one expressed by typical Cu^I–bisdiimine complexes as it is more tetragonally distorted than in the solid state. Furthermore, the phenyl rings of the ligand are almost perpendicular to the diimine central skeleton in the solid state, whereas in solution this angle is predicted to be 59.0°. The two Cu–N bonds between the nitrogen atoms of a chelating ligand and the Cu^I center are almost equal, and the dihedral angle between the two diimines is 65.5°.

As can be seen in Figure 9, the highest occupied molecular orbital (HOMO) of this molecule is of a d–σ* nature and comprises an almost equal contribution from the metal and the diimine regions. The lowest unoccupied molecular orbital (LUMO) is mainly located in the diazabutadiene region of the ligand with small participation of the naphthyl moiety and the metal core and accommodates a bonding character between the carbon atoms of the diazabutadiene and an antibonding character for the two imine bonds. The picture for the HOMO–1 and LUMO+1 is analogous and the HOMO–1 has contributions from the phenyl pendant rings. Further frontier molecular orbitals (FMOs) are given in the Supporting Information. Taking into account that the orbitals that are mainly expected to be involved in the

 © 2013 Wiley-VCH Verlag GmbH & Co. KGaA, Weinheim

low-energy excitations of the system are localized in the diiminic region, a mixing between them and not a clear spatial separation would be expected to characterize the charge transfer (CT) bands of the system. This feature explains in part the enhanced intensity of the absorption of the complexes assigned as MLCT with a potent admixture of intraligand (IL) character. The CT character of this transition can be revealed by considering mainly the higher virtual MOs located in the naphthyl part (see Supporting Information), which will also be involved in these transitions and result in a charge displacement from the region of the Cu^{I} center. Additionally, the mixing that seems to exist between the highest occupied and the lowest virtual MOs of the system in conjunction with the impure atomic orbital origin of mainly the HOMO and HOMO–1, as they comprise a partial metallic and a partial diimine character, can result in a potent noninnocent character for the complexes and this compromises with their complicated electrochemical behavior. Finally, considering that the lowest lying MLCT state of these molecules will mainly arise from electronic transitions between the highest occupied and the lowest unoccupied MOs (Figure 9), a highly delocalized nature and an increased stabilization[43–48] for this state is expected, which supports the lack of emission according to the energy gap law and also renders this state with an impure charge-transfer character. Time resolved studies of the excited state dynamics of these molecules are underway to unravel the impact of the above delocalized character of the CT states on the electron relaxation pathways of the compounds.

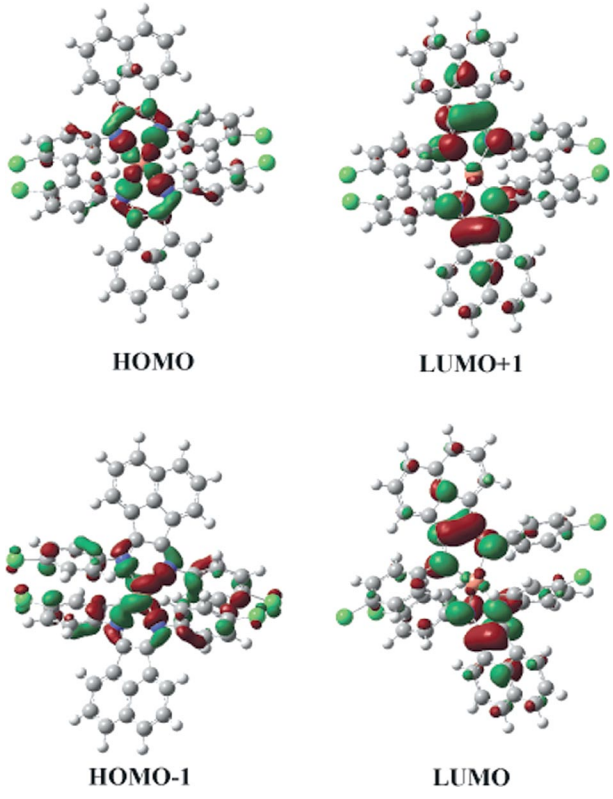

Figure 9. FMOs of the optimized structure of $[Cu(\mathbf{3})_2]^+$ in dichloromethane solution.

Another point that has to be emphasized is the influence of the phenyl ring substituents on the energy of the MLCT bands of the complexes. As is obvious from the shape of the FMOs in Figure 9, the π system of these rings is strongly involved in the HOMO–1 and so the substituent will have an energetic impact on it. The participation of the phenyl rings on the excitations should be expected owing to their free rotation in solution. Alternatively, the differences in the form and energy of the visible absorption of the complexes further support this hypothesis as the lack of electronic communication between the substituted rings and the main acenapthene skeleton would result in absorption spectra with minor variations between the complexes. Therefore, the energy changes of the MLCT absorption when the substitution pattern is altered will mainly be expressed through a change in the energy of the HOMO–1 and this can offer a further explanation for the substantially redshifted MLCT absorption of $[Cu(\mathbf{1})_2]BF_4$, for which the strong donor ability of the *p*-MeO group will raise the energy of its HOMO–1 and reduce the respective energy gap with the associated virtual orbitals.

Conclusions

A new family of Cu^{I}–bisdiimine complexes bearing redox active Ar-BIAN ligands has been synthesized and characterized. Ligand **5** is new and its synthesis, as well as that of the other studied ligands, is achieved by a modified procedure in which extremely dry conditions are not required. The complexes appear to possess a tetrahedral copper environment, and the complex with the *p*-chloro-substituted Ar-BIAN ligand is a rare example of an almost symmetrical complex with two identical chelating ligands. The *o*-phenyl derivative offers an example of an extremely crowded coordination environment in which the carbon atoms are all nonequivalent even in solution.

Despite the well-known noninnocent character of the donors when combined with certain metal centers, Cu^{I} seems to preserve its oxidation state in these complexes and the Ar-BIAN molecules remain in their closed-shell neutral oxidation state. The extended π system of the acenaphthenequinone skeleton induces an enhanced absorption in the visible part of the spectrum and into the NIR region and thus improves the light-gathering characteristics of the complexes. Although no emission was observed in the visible region, it could not be excluded for wavelengths greater than 900 nm as the lack of appropriate equipment did not allow us to investigate such a hypothesis. Additionally, in a series of time-resolved absorption studies performed for these complexes, which be published in a subsequent paper, the lifetime of their lowest excited state is still sufficient for bimolecular processes to occur. In conjunction with the strong absorption features of the complexes in the 500–600 nm region, the compounds can be regarded as attractive candidates for a number of energy-conversion applications such as dopant chromophores in organic solar cells. The absorption characteristics of the complexes follow

 © 2013 Wiley-VCH Verlag GmbH & Co. KGaA, Weinheim

those of the related bis-phenanthroline systems and in combination with the well-known ability of the ligands to stabilize radical and anionic species they could result in a family of potent photo-oxidizers through a possible reductive quenching[49,50] of their MLCT excited states. As has already been reported by Miller and Karpishin, the expansion of the absorption of Cu^{I}–bisdiimine systems in the NIR region necessitates a severe flattening distortion in their ground state. In the same context, the use of highly conjugated organic skeletons coordinated to the metal center leads to an extended delocalization, which brings the energy of the excited MLCT state rather close to that of the ground state. Both the above characteristics result in poor photophysical behavior of the systems. In the present case, the capacity of the complexes to absorb up to the NIR region, even though with low ε values, seems mainly to stem from the enhanced mixing of their FMOs, which results in a highly delocalized nature of their MLCT excited state and a lack of emission at least in the visible part of the spectrum, in accordance with Miller and Karpishin's remarks.[4] To the best of our knowledge, these complexes are rare examples of Cu^{I} systems that absorb light up to 900 nm.

The absorption spectra of the complexes in dichloromethane solutions reveal the capacity of the substituents to tune both the intensity and the energy of the MLCT band by affecting mainly the energy level of the HOMO–1 of these molecules. The enhanced absorption intensity observed for these systems stems from orbital mixing between the FMOs and the displacement of charge away from the metal center following the MLCT excitation. Additionally, the mixing of the FMOs as revealed by DFT calculations indicates a potent noninnocent character for these complexes, although without changes in the oxidation states of the metal core and the ligands as is revealed by crystallographic and spectroscopic data. Despite the increased basicity and the π acidity of the ligands, the respective complexes are not stable in strongly coordinating solvents.

Experimental Section

Materials and Measurements: Acenaphthenequinone and the substituted anilines were purchased from ACROS (p.a. grade) and were used without any prior purification. The solvents used were of reagent grade and were not subjected to any further drying process prior to use. Elemental analyses for C, H, and N were performed with a Perkin–Elmer 240B elemental analyzer. Infrared spectra of KBr pellets were recorded with a Perkin–Elmer Spectrum One FTIR spectrometer with a resolution of 2 cm^{-1} following the collection of 16 scans over the range 4000–360 cm^{-1}. Electronic excitation spectra were recorded for samples in dichloromethane in 1 cm cuvettes with a Shimadzu UV-3600 UV/Vis/NIR spectrophotometer with a resolution of 0.1 nm. Emission studies were performed with optically diluted solutions with a Jobin–Yvon Fluorolog-3 Fluorometer. Solution ^{1}H and ^{13}C NMR spectra of $CDCl_3$ solutions were recorded at 300 and 75 MHz, respectively, with a Varian 300 spectrometer and tetramethylsilane (TMS) as internal standard. Differential pulse voltammetry was used for the electrochemical measurements with an Ivium CompactStat potentiostat/galvanostat with an impedance analyzer. Measurements were performed in a one-compartment cell with a silver wire as a pseudo-reference electrode and a glassy carbon auxiliary electrode. A platinum working electrode was used for the measurements. Recordings were carried out in the potential region –2000 to +2000 mV at ambient temperature at a scan rate of 50 $mV\,s^{-1}$. Recrystallized tetrabutylammonium tetrafluoroborate (0.1 M) was used as the electrolyte. All scans were recorded with degassed solvent and with a flow of moisture-free dinitrogen over the solution surface.

Synthesis of the Ligands: The preparation of the investigated Ar-BIAN ligands was the one proposed by Ragaini et al.[11] with some modifications described below. The synthesis was performed in air and in glassware dried overnight at 100 °C. A major difficulty in the process relates to the extremely dry conditions required for the use of $ZnCl_2$ and this was bypassed by forming the ethyl ether complex of $ZnCl_2$, which has been utilized in various organozinc syntheses as intermediate.[51] The procedure applied is efficient regardless of exposure to moist air and the results are comparable to those obtained with fresh anhydrous $ZnCl_2$ samples. In a typical preparation, $ZnCl_2$ (4.4 g, 32.3 mmol) was sonicated in Et_2O (40 mL) in a sealed flask until an almost biphasic emulsion resulted. After the addition of Na_2SO_4, this emulsion was stirred for 20 min and filtered over a flask containing acenaphthenequinone (2.30 g, 12 mmol) stirred in glacial acetic acid (28 mL) at 60 °C. A reflux condenser was attached to the flask, and the suspension was further stirred and heated. When the solvent started to boil, the respective aniline (27.6 mmol) was added, and the flask was left open for about 5 min to allow evaporation of the ether. The mixture was then heated to reflux for an additional 40 min. Filtration of the hot suspension through a Gooch filter produced the $ZnCl_2$(Ar-BIAN) complex. The solid was washed with a portion (5 mL) of glacial acetic acid and two portions of cold Et_2O and dried in air overnight. The purity of this intermediate product was verified by the absence of any absorption in the IR spectrum above 1700 cm^{-1}. If needed, further purification was achieved by suspension of the product for 10 min in a small amount of dichloromethane, filtration, and air drying. For the decomplexation, the Zn complex was dissolved in dichloromethane (200 mL) in a sealed conical flask, into which a solution of potassium oxalate (36 mmol) in water (20 mL) was added. The solution was vigorously stirred for 15 min, and the two phases were separated with a separating funnel. The organic layer was washed with water and dried with Na_2SO_4. Filtration of the organic layer and evaporation to dryness produced the analytically pure ligand in good yield. Alternatively, this decomplexation was carried out by stirring the intermediate complex in aqueous potassium oxalate (36 mmol, 300 mL), into which a few drops of acetone were added, for 20 min. The suspension gradually changed color, which indicated the progress of the decomplexation. The solid was collected by filtration and washed with cold water and methanol to afford the free ligand, which was left to dry in air. This alternative decomplexation does not seem to work for *p*-MeO-BIAN, for which a product with a different IR spectrum compared to that isolated by the conventional route was obtained. This was not investigated further. The addition of the small amount of acetone is essential as several experiments revealed. The analytical data for all of the ligands including the new compound **5** are given below. The isolation yields were comparable to the reported ones.[11]

***p*-MeO-BIAN (1):** Red solid, overall yield 70% (8.40 mmol, 3.30 g). $C_{26}H_{20}N_2O_2$ (392.46): calcd. C 79.57, H 5.14, N 7.14; found C 79.40, H 5.12, N 7.00. IR (KBr): $\tilde{\nu}$ = 3045 (w, =C–H), 2948 (w, –C–H), 1642 (m, C=C), 1617 (m, C=N–), 1600 (w), 1502 (s), 1238 (s), 1030 (s), 835 (s) cm^{-1}. ^{1}H NMR ($CDCl_3$, 300 MHz, 25 °C): δ = 7.88 (d, J = 8 Hz, 2 H), 7.38 (t, J = 7 Hz, 2 H), 7.12–7.07 (m, 4

 © 2013 Wiley-VCH Verlag GmbH & Co. KGaA, Weinheim

H), 7.04–6.99 (m, 6 H), 3.89 (s, 6 H) ppm. $^{13}C\{^1H\}$ NMR ($CDCl_3$, 75 MHz, 25 °C): δ = 161.8, 157.1, 145.1, 141.9, 131.4, 129.1, 128.9, 127.8, 123.9, 120.0, 114.8, 55.7 ppm.

***p*-Me-BIAN (2):** Orange solid, overall yield 72% (8.64 mmol, 3.11 g). $C_{26}H_{20}N_2$ (360.46): calcd. C 86.64, H 5.59, N 7.77; found C 85.96, H 5.62, N 7.67. IR (KBr): $\tilde{\nu}$ = 3051 (w, =C–H), 2914 (w, –C–H), 1655 (m, C=C), 1628 (s, C=N–), 1602 (m), 1500 (s), 1237 (m), 826 (s) cm^{-1}. ^1H NMR ($CDCl_3$, 300 MHz, 25 °C): δ = 7.87 (d, J = 8 Hz, 2 H), 7.37 (t, J = 7 Hz, 2 H), 7.26 (d, J = 7 Hz, 4 H), 7.05–7.01 (tt, 4 H), 6.92 (d, J = 7 Hz, 2 H), 2.4 (s, 6 H) ppm. $^{13}C\{^1H\}$ NMR ($CDCl_3$, 75 MHz, 25 °C): δ = 161.5, 149.4, 141.9, 134.1, 131.4, 130.2, 129.0, 128.9, 127.8, 124.1, 118.4, 21.3 ppm.

***p*-Cl-BIAN (3):** Orange solid, overall yield 76% (9.12 mmol, 3.66 g). $C_{24}H_{14}Cl_2N_2$ (401.29): calcd. C 71.83, H 3.52, N 6.98; found C 71.24, H 3.63, N 6.86. IR (KBr): $\tilde{\nu}$ = 3052 (w, =C–H), 1652 (m, C=C), 1629 (m, C=N–), 1619 (m), 1478 (s), 1240 (s), 1089 (s), 839 (s) cm^{-1}. ^1H NMR ($CDCl_3$, 300 MHz, 25 °C): δ = 7.93 (d, J = 8 Hz, 2 H), 7.47–7.40 (m, 6 H), 7.09–7.05 (m, 4 H), 6.96 (d, J = 7 Hz, 2 H) ppm. $^{13}C\{^1H\}$ NMR ($CDCl_3$, 75 MHz, 25 °C): δ = 161.9, 150.2, 142.1, 131.5, 130.1, 129.9, 129.6, 128.4, 128.0, 124.3, 119 ppm.

***o*-Ph-BIAN (4):** Red solid, overall yield 71% (8.52 mmol, 4.13 g). $C_{36}H_{24}N_2$ (484.60): calcd. C 89.23, H 4.99, N 5.78; found C 88.97, H 5.17, N 5.64. IR (KBr): $\tilde{\nu}$ = 3053 (w, =C–H), 1664 (m, C=C), 1633 (m, C=N), 1589 (m), 1473 (s), 1427 (s), 1232 (m), 830 (s), 734 (s), 699 (s) cm^{-1}. ^1H NMR ($CDCl_3$, 300 MHz, 25 °C): δ = 7.8 (d, J = 8 Hz, 2 H), 7.5 (d, J = 7 Hz, 2 H), 7.44–7.40 (m, 5 H), 7.38–7.34 (dd, J = 7 Hz, 2 H), 7.32–7.29 (m, 2 H), 7.26 (q, J = 7 Hz, 2 H), 7.15 (m, 5 H), 7.3 (d, J = 7 Hz, 2 H), 6.8 (d, J = 7 Hz, 2 H) ppm. $^{13}C\{^1H\}$ NMR ($CDCl_3$, 75 MHz, 25 °C): δ = 160.9, 149.7, 141.5, 139.4, 131.3, 131.1, 130.9, 129.7, 129.3, 129.2, 128.9, 128.6, 128.2, 128.1, 127.9, 126.9, 125.0, 123.6, 118.8 ppm.

***m*-Cl-BIAN (5):** Yellow solid, overall yield 73% (8.76 mmol, 3.52 g). $C_{24}H_{14}Cl_2N_2$ (401.29): calcd. C 71.83, H 3.52, N 6.98; found C 71.22, H 3.63, N 6.89. IR (KBr): $\tilde{\nu}$ = 3047 (m, =C–H), 1668 (s, C=C), 1630 (s, C=N–), 1589 (s), 1466 (s), 1416 (m), 1234 (m), 938 (s), 827 (s), 774 (s) cm^{-1}. ^1H NMR ($CDCl_3$, 300 MHz, 25 °C): δ = 7.96 (d, J = 8 Hz, 2 H), 7.46–7.38 (q, J = 7 Hz, 4 H), 7.27–7.23 (m, J = 7 Hz, 2 H), 7.14 (t, J = 8 Hz, 2 H), 7.04–6.99 (m, 2 H), 6.92 (d, J = 7 Hz, 2 H) ppm. $^{13}C\{^1H\}$ NMR ($CDCl_3$, 75 MHz, 25 °C): δ = 161.9, 152.9, 142.2, 135.3, 131.5, 130.9, 129.7, 128.3, 128.1, 124.8, 124.4, 118.6, 116.7 ppm.

***m*-CF_3-BIAN (6):** Yellow solid, overall yield 72% (8.64 mmol, 4.05 g). $C_{26}H_{14}F_6N_2$ (468.40): calcd. C 66.67, H 3.01, N 5.98; found C 66.44, H 3.15, N 5.87. IR (KBr): $\tilde{\nu}$ = 3060 (w, =C–H), 1669 (m, C=C), 1644 (m, C=N–), 1604 (m), 1592 (m), 1434 (m), 1324 (s), 1176 (s), 1123 (s), 1123 (s), 940 (s), 776 (s) cm^{-1}. ^1H NMR ($CDCl_3$, 300 MHz, 25 °C): δ = 7.95 (d, J = 8 Hz, 2 H), 7.64–7.53 (q, J = 7 Hz, 4 H), 7.45–7.40 (q, J = 7 Hz, 4 H), 7.33 (d, J = 7 Hz, 2 H), 6.84 (d, J = 7 Hz, 2 H) ppm. $^{13}C\{^1H\}$ NMR ($CDCl_3$, 75 MHz, 25 °C): δ = 162.04, 151.98, 142.29, 132.42, 131.99, 131.58, 130.35, 129.88, 128.19, 128.11, 125.98, 124.18, 122.37, 121.94, 121.56, 121.45, 121.41, 115.64, 115.53 ppm.

Synthesis of the Cu^I Complexes: The synthesis of the Cu^I complexes was carried out according to the following general procedure: An appropriate amount of $[Cu(MeCN)_4]BF_4$ (0.5 mmol) was added to a solution of the Ar-BIAN ligand (1.0 mmol) in CH_2Cl_2 (25 mL). The mixture was stirred for 2 h under an Ar atmosphere. The complex forms instantly as indicated by the sudden color change of the solution to dark purple, blue, or green depending on the substitution of the ligand. The solution was filtered, and the filtrate was left to evaporate in air after the addition of Et_2O (3 mL) to afford the final products. Crystals of $[Cu(\mathbf{2})_2]BF_4$ and $[Cu(\mathbf{3})_2]BF_4$ suitable for X-ray analysis were obtained by layering diethyl ether over CH_2Cl_2 solutions of the complexes and slow evaporation at room temperature. For $[Cu(\mathbf{4})_2]BF_4$, $CHCl_3$ was used instead of CH_2Cl_2. For $[Cu(\mathbf{1})_2]BF_4$ and $[Cu(\mathbf{3})_2]BF_4$, broad ^1H NMR signals in $CDCl_3$ were recorded, which indicates that the compounds undergo conformational changes in solution.

$[Cu(\mathbf{1})_2]BF_4$: Dark solid, overall yield 89% (0.45 mmol, 0.46 g). $C_{52}H_{40}BCuF_4N_4O_4{\cdot}CH_2Cl_2$: calcd. C 62.40, H 4.15, N 5.49; found C 62.50, H 4.19, N 5.51. IR (KBr): $\tilde{\nu}$ = 3047 (w, =C–H), 2927 (w, –C–H), 1634 (m, C=N–), 1599 (m), 1504 (m), 1298 (m), 1246 (s), 1053 (s), 1028 (s), 830 (s) cm^{-1}. ^1H NMR ($CDCl_3$, 300 MHz, 25 °C): δ = 8.07 (br d, J = 8 Hz, 2 H), 7.48 (br t, J = 8 Hz, 4 H), 7.26–7.03 (br m, 8 H), 3.90 (s, 3 H) ppm. $^{13}C\{^1H\}$ NMR ($CDCl_3$, 75 MHz, 25 °C): δ = 163.0, 159.4, 142.5, 140.2, 131.5, 131.2, 128.7, 127.0, 124.4, 122.8, 115.3, 56.0 ppm.

$[Cu(\mathbf{2})_2]BF_4$: Dark solid, overall yield 93% (0.47 mmol, 0.45 g). $C_{52}H_{40}BCuF_4N_4{\cdot}CH_2Cl_2$: calcd. C 66.57, H 4.43, N 5.86; found C 66.62, H 4.48, N 5.83. IR (KBr): $\tilde{\nu}$ = 3050 (w, =C–H), 2919 (w, –C–H), 1636 (m, C=N–), 1597 (m), 1488 (s), 1288 (m), 1057 (s), 830 (s) cm^{-1}. ^1H NMR ($CDCl_3$, 300 MHz, 25 °C): δ = 8.09 (d, J = 8 Hz, 2 H), 7.51 (t, J = 7 Hz, 2 H), 7.33–7.29 (m, 6 H), 7.05 (d, J = 8 Hz, 4 H), 2.46 (s, 6 H) ppm. $^{13}C\{^1H\}$ NMR ($CDCl_3$, 75 MHz, 25 °C): δ = 163.8, 145.1, 142.9, 138.0, 131.5, 131.4, 130.9, 128.7, 126.7, 124.8, 120.7, 21.5 ppm.

$[Cu(\mathbf{3})_2]BF_4$: Dark solid, overall yield 91% (0.46 mmol, 0.48 g). $C_{48}H_{28}BCl_4CuF_4N_4{\cdot}CH_2Cl_2$: calcd. C 56.71, H 2.91, N 5.40; found C 56.63, H 2.91, N 5.44. IR (KBr): $\tilde{\nu}$ = 3089 (w, =C–H), 1644 (s, C=N–), 1604 (m), 1482 (s), 1290 (s), 1250 (s), 1085 (s), 1053 (s), 1010 (s), 829 (s), 775 (s) cm^{-1}. ^1H NMR ($CDCl_3$, 300 MHz, 25 °C): δ = 8.07 (br pd), 7.45 (br), 7.21 (br), 7.05 (br) ppm. $^{13}C\{^1H\}$ NMR ($CDCl_3$, 75 MHz, 25 °C): δ = 163.4, 145.7, 141.8, 131.2, 130.9, 129.8, 128.6, 126.2, 126.0, 123.9, 122.5 ppm.

$[Cu(\mathbf{4})_2]BF_4$: Dark solid, overall yield 88% (0.44 mmol, 0.49 g). $C_{72}H_{48}BCuF_4N_4$ (1119.55): calcd. C 77.24, H 4.32, N 5.00; found C 76.83, H 4.19, N 4.88. IR (KBr): $\tilde{\nu}$ = 3055 (w, =C–H), 1637 (m, C=N–), 1593 (m), 1472 (s), 1429 (s), 1284 (m), 1050 (s), 830 (s) 776(s), 764 (s), 740 (s), 700 (s) cm^{-1}. ^1H NMR ($CDCl_3$, 300 MHz, 25 °C): δ = 8.08–7.93 (m), 7.54–6.86 (m), 6.86–6.65 (m) ppm. $^{13}C\{^1H\}$ NMR ($CDCl_3$, 75 MHz, 25 °C): δ = 165.6, 164.6, 164.2, 145.1, 144.3, 142.4, 141.8, 137.9, 133.8, 133.2, 133.0, 132.2, 131.6, 131.0, 129.5, 128.8, 128.7, 128.1, 127.8, 127.4, 126.5, 125.1, 123.0, 121.9 ppm.

$[Cu(\mathbf{5})_2]BF_4$: Brown solid, overall yield 92% (0.46 mmol, 0.44 g). $C_{48}H_{28}BCl_4CuF_4N_4$ (952.94): calcd. C 60.50, H 2.96, N 5.88; found C 59.95, H 3.10, N 5.64. IR (KBr): $\tilde{\nu}$ = 3066 (w, =C–H), 1637 (m, C=N–), 1584 (s), 1469 (s), 1420 (s), 1280 (s), 1059 (s), 829 (s), 776 (s), 688 (s) cm^{-1}. ^1H NMR ($CDCl_3$, 300 MHz, 25 °C): δ = 8.14 (d, J = 8 Hz, 2 H), 7.62–7.53 (m, 4 H), 7.43 (d, J = 8 Hz, 2 H), 7.24 (d, J = 8 Hz, 2 H), 7.15 (d, J = 8 Hz, 2 H) 7.07 (s, 2 H) ppm. $^{13}C\{^1H\}$ NMR ($CDCl_3$, 75 MHz, 25 °C): δ = 165.0, 148.5, 143.5, 136.0, 132.2, 132.1, 131.6, 129.0, 128.1, 126.0, 125.4, 120.6, 119.2 ppm.

$[Cu(\mathbf{6})_2]BF_4$: Dark solid, overall yield 91% (0.46 mmol, 0.54 g). $C_{52}H_{28}BCuF_{16}N_4{\cdot}CH_2Cl_2$: calcd. C 54.31, H 2.58, N 4.78; found C 54.52, H 2.65, N 5.04. IR (KBr): $\tilde{\nu}$ = 3074 (w, =C–H), 1644 (m, C=N–), 1587 (m), 1487 (m), 1438 (m), 1327 (m), 1182 (s) 1166 (s), 1126 (s), 1066 (s), 1049 (s), 778 (s), 697 (s), 662 (s) cm^{-1}. ^1H NMR ($CDCl_3$, 300 MHz, 25 °C): δ = 8.13 (d, J = 8 Hz, 2 H), 7.85 (t, J = 8 Hz, 2 H), 7.72 (d, J = 8 Hz, 2 H), 7.53 (t, J = 8 Hz, 4 H), 7.36

 © 2013 Wiley-VCH Verlag GmbH & Co. KGaA, Weinheim

Table 5. Crystallographic data and refinement details for $[Cu(\mathbf{2})_2]BF_4 \cdot 1.5CH_2Cl_2$, $[Cu(\mathbf{3})_2]BF_4$, and $[Cu(\mathbf{4})_2]BF_4 \cdot 3CHCl_3$.

	$[Cu(\mathbf{2})_2]BF_4 \cdot 1.5CH_2Cl_2$	$[Cu(\mathbf{3})_2]BF_4$	$[Cu(\mathbf{4})_2]BF_4 \cdot 3CHCl_3$
Crystal system	monoclinic	orthorhombic	triclinic
Temperature [K]	120	293	130
Radiation	Mo-K_α	Cu-K_α	Cu-K_α
Space group	$C2/c$	$Ccca$	$P\bar{1}$
a [Å]	38.145(5)	14.1998(11)	a = 11.8970(5)
b [Å]	14.461(1)	21.9723(14)	b = 15.5900(7)
c [Å]	19.864(2)	14.9553(11)	c = 18.5407(7)
α [°]	90	90	α = 99.743(3)
β [°]	121.76(2)	90	β = 91.870(3)
γ [°]	90	90	γ = 94.147(3)
Volume [Å^3]	9316.5(17)	4666.1(6)	3376.8(2)
Z, Z'	8, 1	4, 0.25	2, 1
Absorption coefficient	0.700	3.214	4.213
Reflections collected	52588	7603	49932
Independent reflections	8200	2071	13800
Completeness to θ (max.)	99.6%	99.9%	99.8%
Data/restraints/parameters	8200/0/614	2071/0/143	13800/6/885
Goodness- of-fit on F^2	1.040	1.105	1.044
Final R indices [$I > 2\sigma(I)$]	R_1 = 0.0706, wR_1 = 0.1329	R_1 = 0.0537, wR_1 = 0.1465	R_1 = 0.0545, wR_1 = 0.1453
R indices (all data)	R_2 = 0.1217, wR_2 = 0.1556	R_2 = 0.0656, wR_2 = 0.1570	R_1 = 0.0582, wR_1 = 0.1485
Largest diff. peak and hole	0.68, –0.90	0.55, –0.38	0.76, –1.04

(s, 2 H), 7.10 (d, J = 8 Hz, 2 H) ppm. $^{13}C\{^1H\}$ NMR ($CDCl_3$, 75 MHz, 25 °C): δ = 165.2, 147.6, 143.5, 132.8, 132.4, 132.0, 131.4, 128.8, 125.8, 125.2, 125.0, 124.4, 121.6, 116.8 ppm.

X-ray Crystal Structure: The diffraction data were collected with Oxford Diffraction Xcalibur E ($[Cu(\mathbf{2})_2]BF_4 \cdot 1.5CH_2Cl_2$) or SuperNova A ($[Cu(\mathbf{3})_2]BF_4$ and $[Cu(\mathbf{4})_2]BF_4 \cdot 3CHCl_3$) CCD diffractometers. Data collection and reduction were performed with the CrysAlis software.[52] The structures were solved by direct methods with the SHELXS-97 program[53] and refined by full-matrix least-squares method on F^2 with SHELXL-97. The hydrogen atoms from C–H groups were placed in idealized positions and refined by using a riding model. $[Cu(\mathbf{2})_2]BF_4 \cdot 1.5CH_2Cl_2$ and $[Cu(\mathbf{4})_2]BF_4 \cdot 3CHCl_3$ contain disordered solvent molecules. Additional details concerning crystal data and structure refinement are given in Table 5. Selected bond lengths and angles are listed in Table 3. Molecular graphics were generated with ORTEP-3 for Windows[54] and Mercury 2.2 software.[55]

CCDC-873388 (for $[Cu(\mathbf{2})_2]BF_4 \cdot 1.5CH_2Cl_2$), -873389 (for $[Cu(\mathbf{3})_2]BF_4$), and -909212 (for $[Cu(\mathbf{4})_2]BF_4 \cdot 3CHCl_3$) contain the supplementary crystallographic data for this paper. These data can be obtained free of charge from The Cambridge Crystallographic Data Centre via www.ccdc.cam.ac.uk/data_request/cif.

Computational Details: The geometry obtained from the X-ray analysis of the *p*-Cl substituted complex $[Cu(\mathbf{3})_2]BF_4$ was used as the initial point for the optimization of its geometry without any symmetry constraints. DFT calculations were carried out with the Gaussian 03[56] software package with the PCM[42] algorithm implemented in it. Vibrational frequency calculations ensured that the obtained geometry was a real minimum. Becke's three-parameter hybrid exchange functional[57] and the Lee–Yang–Parr nonlocal correlation functional[58] (B3LYP) was used in combination with the 6-31G(d)[59] basis set for the light elements (C, H, N, and Cl), and the LanL2DZ[60] basis set was used for the metal core. Visualization of the FMOs of interest was done with GaussView 4.1.

Supporting Information (see footnote on the first page of this article): Table of Cartesian coordinates of the DFT calculation (Table S1), table of DPV potentials (Table S2), ^1H and ^{13}C NMR spectra (Figures S1–S24), voltamograms of ligands and complexes (Figures S25–S30), absorption spectra of ligands and complexes (Figures S31 and S32), additional FMOs of the cationic unit optimized (Figure S33).

Acknowledgments

P. P. acknowledges support by the Centre for International Mobility of Finland (CIMO) under grant TM-11-7670. The authors would like to thank Alexander Efimov and Vladimir Chukharev at Tampere for their support throughout the project and Dr. Anastasios Papadopoulos at AUTH for his graphical work.

[1] a) A. S. Polo, M. K. Itokazu, N. Y. Murakami Iha, *Coord. Chem. Rev.* **2004**, *248*, 1343–1361; b) M.-F. Charlot, Y. Pellegrin, A. Quaranta, W. Leibl, A. Aukauloo, *Chem. Eur. J.* **2006**, *12*, 796–812; c) A. Anthonysamy, Y. Lee, B. Karunagaran, V. Ganapathy, S.-W. Rhee, S. Karthikeyan, K. S. Kim, M. J. Ko, N.-G. Park, M.-J. Ju, J. K. Kim, *J. Mater. Chem.* **2011**, *21*, 12389–12397; d) H. Choi, C. Baik, S. Kim, M.-S. Kang, X. Xu, H. S. Kang, S. O. Kang, J. Ko, Md. K. Nazeeruddin, M. Grätzel, *New J. Chem.* **2008**, *32*, 2233–2237; e) J. N. Clifford, E. Martínez-Ferrero, A. Viterisi, E. Palomares, *Chem. Soc. Rev.* **2011**, *40*, 1635–1646; f) B. W. D'Andrade, R. J. Holmes, S. R. Forrest, *Adv. Mater.* **2004**, *16*, 624–628; g) V. Balzani, G. Bergamini, P. Ceroni, *Coord. Chem. Rev.* **2008**, *252*, 2456–2469; h) P.-T. Chou, Y. Chi, M.-W. N. Chung, C.-C. Lin, *Coord. Chem. Rev.* **2011**, *255*, 2653–2665; i) T. N. Singh-Rachford, F. N. Castellano, *Coord. Chem. Rev.* **2010**, *254*, 2560–2573.

[2] a) S. Fantacci, F. De Angelis, *Coord. Chem. Rev.* **2011**, *255*, 2704–2726; b) S. Fraysse, C. Coudret, J.-P. Launay, *J. Am. Chem. Soc.* **2003**, *125*, 5880–5888; c) V. Balzani, G. Bergamini, F. Marchioni, P. Ceroni, *Coord. Chem. Rev.* **2006**, *250*, 1254–1266; d) C. Olivier, B. S. Kim, D. Touchard, S. Rigaut, *Organometallics* **2008**, *27*, 509–518; e) P. P. Lainé, S. Campagna, F. Loiseau, *Coord. Chem. Rev.* **2008**, *252*, 2552–2571; f) J. K. Barton, E. D. Olmon, P. A. Sontz, *Coord. Chem. Rev.* **2011**, *255*, 619–634.

[3] a) Q. Zhang, J. Ding, Y. Cheng, L. Wang, Z. Xie, X. Jing, F. Wang, *Adv. Funct. Mater.* **2007**, *17*, 2983–2990; b) Q. Zhang, Q. Zhou, Y. Cheng, L. Wang, D. Ma, X. Jing, F. Wang, *Adv. Mater.* **2004**, *16*, 432–436; c) N. Armaroli, G. Accorsi, M. Hol-

 © 2013 Wiley-VCH Verlag GmbH & Co. KGaA, Weinheim

ler, O. Moudam, J.-F. Nierengarten, Z. Zhou, R. T. Wegh, R. Welter, *Adv. Mater.* **2006**, *18*, 1313–1316; d) B. Bozic-Weber, E. C. Constable, C. E. Housecroft, M. Neuburger, J. R. Price, *Dalton Trans.* **2010**, *39*, 3585–3594; e) H. Yersin, R. F. Rausch, R. Czerwieniec, T. Hofbeck, T. Fischer, *Coord. Chem. Rev.* **2011**, *255*, 2622–2652; f) R. Barbieri, G. Accorsi, N. Armaroli, *Chem. Commun.* **2008**, 2185–2193; g) T. Bessho, E. C. Constable, M. I. Graetzel, A. Hernandez Redondo, C. E. Housecroft, W. Kylberg, Md. K. Nazeeruddin, M. Neuburger, S. Schaffner, *Chem. Commun.* **2008**, 3717–3719; h) O. Moudam, A. Kaeser, B. Delavaux-Nicot, C. Duhayon, M. Holler, G. Accorsi, N. Armaroli, I. Séguy, J. Navarro, P. Destruel, J.-F. Nierengarten, *Chem. Commun.* **2007**, 3077–3079.

[4] M. T. Miller, T. B. Karpishin, *Inorg. Chem.* **1999**, *38*, 5246–5249.

[5] a) R. van Asselt, C. J. Elsevier, *J. Mol. Catal. A* **1991**, *65*, L13; b) D. J. Tempel, L. K. Johnson, R. L. Huff, P. S. White, M. Brookhart, *J. Am. Chem. Soc.* **2000**, *122*, 6686–6700; c) D. B. Llewellyn, D. Adamson, B. A. Arndtsen, *Org. Lett.* **2000**, *2*, 4165–4168; d) P. A. Evans, V. S. Murthy, J. D. Roseman, A. L. Rheingold, *Angew. Chem.* **1999**, *111*, 3370; *Angew. Chem. Int. Ed.* **1999**, *38*, 3175–3177; e) S. Cenini, F. Ragaini, S. Tollari, D. Paone, *J. Am. Chem. Soc.* **1996**, *118*, 11964–11965; f) F. Ragaini, S. Cenini, S. Tollari, G. Tummolillo, R. Beltrami, *Organometallics* **1999**, *18*, 928–942.

[6] G. Knör, M. Leirer, T. E. Keyes, J. G. Vos, A. Vogler, *Eur. J. Inorg. Chem.* **2000**, 749–751.

[7] a) H. L. Wong, L. S. M. Lam, K. W. Cheng, K. Y. K. Man, W. K. Chan, C. Y. Kwong, A. B. Djurišić, *Appl. Phys. Lett.* **2004**, *84*, 2557; b) C. S. K. Mak, H. Wong, Q. Y. Leung, W. Y. Tam, W. K. Chan, A. B. Djurišić, *J. Organomet. Chem.* **2009**, *694*, 2770–2776; c) W. K. Chan, C. S. Hui, K. Y. K. Man, K. W. Cheng, H. L. Wong, N. Zhu, A. B. Djurišić, *Coord. Chem. Rev.* **2005**, *249*, 1351–1359.

[8] I. L. Fedushkin, A. S. Nikipelov, A. A. Skatova, O. V. Maslova, A. N. Lukoyanov, G. K. Fukin, A. V. Cherkasov, *Eur. J. Inorg. Chem.* **2009**, 3742–349.

[9] I. L. Fedushkin, A. A. Skatova, V. K. Cherkasov, V. A. Chudakova, S. Dechert, M. Hummert, H. Schumann, *Chem. Eur. J.* **2003**, *9*, 5778–5783.

[10] a) I. L. Fedushkin, A. N. Lukoyanov, S. Y. Ketkov, M. Hummert, H. Schumann, *Chem. Eur. J.* **2007**, *13*, 7050–7056; b) I. L. Fedushkin, A. N. Lukoyanov, A. N. Tishkina, G. K. Fukin, K. A. Lyssenko, M. Hummert, *Chem. Eur. J.* **2010**, *16*, 7563–7571; c) H. Schumann, M. Hummert, A. N. Lukoyanov, I. L. Fedushkin, *Organometallics* **2005**, *24*, 3891–3896; d) M. Gasperini, F. Ragaini, *Organometallics* **2004**, *23*, 995–1001; e) D. H. Camacho, E. V. Salo, Z. Guan, J. W. Ziller, *Organometallics* **2005**, *24*, 4933–4939; f) J. C. Alonso, P. Neves, M. J. P. da Silva, S. Quintal, P. D. Vaz, C. Silva, A. A. Valente, P. Ferreira, M. J. Calhorda, V. Félix, M. G. B. Drew, *Organometallics* **2007**, *26*, 5548–5556; g) A. Scarel, M. Rosa Axet, F. Amoroso, F. Ragaini, C. J. Elsevier, A. Holuigue, C. Carfagna, L. Mosca, B. Milani, *Organometallics* **2008**, *27*, 1486–1494; h) C. S. Popeney, A. L. Rheingold, Z. Guan, *Organometallics* **2009**, *28*, 4452–4463; i) I. L. Fedushkin, A. A. Skatova, V. A. Chudakova, G. K. Fukin, *Angew. Chem.* **2003**, *115*, 3416; *Angew. Chem. Int. Ed.* **2003**, *42*, 3294–3298; j) I. L. Fedushkin, A. A. Skatova, V. A. Chudakova, V. K. Cherkasov, G. K. Fukin, M. A. Lopatin, *Eur. J. Inorg. Chem.* **2004**, 388–393; k) I. L. Fedushkin, V. M. Makarov, V. G. Sokolov, G. K. Fukin, *Dalton Trans.* **2009**, 8047–8053; l) M. M. Khusniyarov, K. Harms, O. Burghaus, J. Sundermeyer, *Eur. J. Inorg. Chem.* **2006**, 2985–2996.

[11] M. Gasperini, F. Ragaini, S. Cenini, *Organometallics* **2002**, *21*, 2950–2957.

[12] U. El-Ayaan, F. Murata, S. El-Derby, Y. Fukuda, *J. Mol. Struct.* **2004**, *692*, 209–216.

[13] I. L. Fedushkin, V. A. Chudakova, A. A. Skatova, N. M. Khvoinova, Y. A. Kurskii, T. A. Glukhova, G. K. Fukin, S. Dechert, M. Hummert, H. Schumann, *Z. Anorg. Allg. Chem.* **2004**, *630*, 501–507.

[14] M. D. Ward, J. A. McCleverty, *J. Chem. Soc., Dalton Trans.* **2002**, 275–288.

[15] P. Chaudhuri, C. N. Verani, E. Bill, E. Bothe, T. Weyhermüller, K. Wieghardt, *J. Am. Chem. Soc.* **2001**, *123*, 2213–2223.

[16] D. N. Coventry, R. S. Batsanov, R. E. Goeta, J. A. K. Howard, T. B. Marder, *Polyhedron* **2004**, *23*, 2789–2795.

[17] U. El-Ayaan, A. Paulovicova, Y. Fukuda, *J. Mol. Struct.* **2003**, *645*, 205–212.

[18] T. Kern, U. Monkowius, M. Zabel, G. Knör, *Inorg. Chim. Acta* **2011**, *374*, 632–636.

[19] H. A. Jenkins, C. L. Dumaresque, D. Vidovic, J. A. C. Clyburne, *Can. J. Chem.* **2002**, *80*, 1398–1403.

[20] V. Rosa, T. Avilés, G. Aullon, B. Covelo, C. Lodeiro, *Inorg. Chem.* **2008**, *47*, 7734–7744 and references cited therein.

[21] S. B. Singh, K. N. Mehrotra, *Can. J. Chem.* **1982**, *60*, 1901–1906.

[22] K. Vasudevan, A. H. Cowley, *Chem. Commun.* **2007**, 3464–3466.

[23] I. L. Fedushkin, A. A. Skatova, V. A. Chudakova, N. M. Khvoinova, A. Yu. Baurin, *Organometallics* **2004**, *23*, 3714–3718.

[24] A. N. Chebotarev, M. V. Shestakova, T. M. Shcherbakova, *Russ. J. Coord. Chem.* **2002**, *28*, 131–134.

[25] M. Gasperini, F. Ragaini, E. Gazzola, A. Caselli, P. Macchi, *Dalton Trans.* **2004**, 3376–3382, and references cited therein.

[26] The two species are in equilibrium and the removal of the *anti–anti* isomer through coordination with a metal center would favour the total conversion of the *syn–anti* isomer to the *anti–anti* isomer.

[27] a) R. van Asselt, C. J. Elsevier, C. Amatore, A. Jutand, *Organometallics* **1997**, *16*, 317–328; b) G. J. Stor, F. Hartl, J. W. M. van Outersterp, D. J. Stufkens, *Organometallics* **1995**, *14*, 1115–1100; c) A. Paulovicova, U. El-Ayaan, K. Umezawa, C. Vithana, Y. Ohashi, Y. Fukuda, *Inorg. Chim. Acta* **2002**, *339*, 209–214.

[28] A. K. Ichinaga, J. R. Kirchhoff, D. R. McMillin, C. O. Dietrich-Buchecker, P. A. Marnot, J. P. Sauvage, *Inorg. Chem.* **1987**, *26*, 4290–4292.

[29] C. C. Phifer, D. R. McMillin, *Inorg. Chem.* **1986**, *25*, 1329–1333.

[30] R. M. Everly, D. R. McMillin, *J. Phys. Chem.* **1991**, *95*, 9071–9075.

[31] C. T. Cunningham, K. L. H. Cunningham, J. F. Michalec, D. R. McMillin, *Inorg. Chem.* **1999**, *38*, 4388–4392.

[32] M. T. Miller, P. K. Gantzel, T. B. Karpishin, *Inorg. Chem.* **1999**, *38*, 3414–3422.

[33] V. Kalsani, M. Schmittel, R. Listorti, G. Accorsi, N. Armaroli, *Inorg. Chem.* **2006**, *45*, 2061–2067.

[34] N. Armaroli, G. Accorsi, F. Cardinali, R. Listorti, *Top. Curr. Chem.* **2007**, *280*, 69–115.

[35] N. Armaroli, *Chem. Soc. Rev.* **2001**, *30*, 113–124.

[36] M. Z. Zgierski, *J. Chem. Phys.* **2003**, *118*, 4045–4051.

[37] O. Green, B. A. Gandhi, J. N. Burstyn, *Inorg. Chem.* **2009**, *48*, 5704–5714.

[38] T. Kern, U. Monkowius, M. Zabel, G. Knör, *Eur. J. Inorg. Chem.* **2010**, 4148–4156.

[39] V. Rosa, C. I. M. Santos, R. Welter, G. Aullón, C. Lodeiro, T. Avilés, *Inorg. Chem.* **2010**, *49*, 8699–8708 and references cited therein.

[40] N. J. Hill, I. Vargas-Baca, A. H. Cowley, *Dalton Trans.* **2009**, 240–253.

[41] L. Li, P. S. Lopes, V. Rosa, C. A. Figueira, M. A. N. D. A. Lemos, M. T. Duarte, T. Avilés, P. T. Gomes, *Dalton Trans.* **2012**, *41*, 5144–5154.

[42] a) S. Miertus, E. Scrocco, J. Tomasi, *Chem. Phys.* **1981**, *55*, 117–129; b) J. Tomasi, M. Persico, *Chem. Rev.* **1994**, *94*, 2027–2094; c) C. Amovilla, V. Barone, R. Cammi, E. Cances, M.

 © 2013 Wiley-VCH Verlag GmbH & Co. KGaA, Weinheim

Cossi, B. Mennucci, C. S. Pomelli, J. Tomasi, *Adv. Quantum Chem.* **1998**, *32*, 227–261.
[43] S. Boyde, G. F. Strouse, W. E. Jones Jr., T. J. Meyer, *J. Am. Chem. Soc.* **1990**, *112*, 7395–7396.
[44] A. C. Benniston, V. Grosshenny, A. Harriman, R. Ziessel, *Angew. Chem.* **1994**, *106*, 1956; *Angew. Chem. Int. Ed. Engl.* **1994**, *33*, 1884–1885.
[45] G. F. Strouse, J. R. Schoonover, R. Duesing, S. Boyde, W. E. Jones Jr., T. J. Meyer, *Inorg. Chem.* **1995**, *34*, 473–487.
[46] V. Grosshenny, A. Harriman, F. Romero, R. Ziessel, *J. Phys. Chem.* **1996**, *100*, 17472–17484.
[47] J. A. Treadway, B. Loeb, R. Lopez, P. A. Anderson, F. R. Keene, T. J. Meyer, *Inorg. Chem.* **1996**, *35*, 2242–2246.
[48] N. H. Damrauer, T. R. Boussie, M. Devenney, J. K. McCusker, *J. Am. Chem. Soc.* **1997**, *119*, 8253–8268.
[49] D. V. Scaltrito, D. W. Thompson, J. A. O'Callaghan, G. J. Meyer, *Coord. Chem. Rev.* **2000**, *208*, 243–266.
[50] M. Ruthkosky, C. A. Kelly, F. N. Castellano, G. J. Meyer, *Coord. Chem. Rev.* **1998**, *171*, 309–322.
[51] D. K. Breitinger, C. E. Zybill, in: *Synthetic methods of organometallic inorganic chemistry* (Eds.: D. K. Breitinger, W. A. Herrmann), Thieme, Stuttgart, Germany, **1999**, vol. 10, chapter 4.3, p. 160–165.
[52] *Crysalis CCD*, *RED*, v. 1.171.31, Oxford Diffraction, Abingdon, UK, **2006**.
[53] G. M. Sheldrick, *Acta Crystallogr., Sect. A* **2008**, *64*, 112–122.
[54] A. L. Spek, *Acta Crystallogr., Sect. D* **2009**, *65*, 148–155.
[55] L. J. Farrugia, *J. Appl. Crystallogr.* **1997**, *30*, 565.
[56] M. J. Frisch, G. W. Trucks, H. B. Schlegel, G. E. Scuseria, M. A. Robb, J. R. Cheeseman, J. A. Montgomery Jr., T. Vreven, K. N. Kudin, J. C. Burant, J. M. Millam, S. S. Iyengar, J. Tomasi, V. Barone, B. Mennucci, M. Cossi, G. Scalmani, N. Rega, G. A. Petersson, H. Nakatsuji, M. Hada, M. Ehara, K. Toyota, R. Fukuda, J. Hasegawa, M. Ishida, T. Nakajima, Y. Honda, O. Kitao, H. Nakai, M. Klene, X. Li, J. E. Knox, H. P. Hratchian, J. B. Cross, C. Adamo, J. Jaramillo, R. Gomperts, R. E. Stratmann, O. Yazyev, A. J. Austin, R. Cammi, C. Pomelli, J. W. Ochterski, P. Y. Ayala, K. Morokuma, G. A. Voth, P. Salvador, J. J. Dannenberg, V. G. Zakrzewski, S. Dapprich, A. D. Daniels, M. C. Strain, O. Farkas, D. K. Malick, A. D. Rabuck, K. Raghavachari, J. B. Foresman, J. V. Ortiz, Q. Cui, A. G. Baboul, S. Clifford, J. Cioslowski, B. B. Stefanov, G. Liu, A. Liashenko, P. Piskorz, I. Komaromi, R. L. Martin, D. J. Fox, T. Keith, M. A. Al-Laham, C. Y. Peng, A. Nanayakkara, M. Challacombe, P. M. W. Gill, B. Johnson, W. Chen, M. W. Wong, C. Gonzalez, J. A. Pople, *Gaussian 03*, rev. E.01-SMP, Gaussian, Inc., Pittsburgh, **2003**.
[57] A. D. Becke, *Phys. Rev. A* **1988**, *38*, 3098–3100.
[58] C. Lee, W. Yang, R. G. Parr, *Phys. Rev. B* **1988**, *37*, 785–789.
[59] a) P. C. Hariharan, J. A. Pople, *Theor. Chim. Acta* **1973**, *28*, 213–222; b) M. M. Francl, W. J. Petro, W. J. Hehre, J. S. Binkley, M. S. Gordon, D. J. DeFrees, J. A. Pople, *J. Chem. Phys.* **1982**, *77*, 3654–3665.
[60] a) P. J. Hay, W. R. Wadt, *J. Chem. Phys.* **1985**, *82*, 270–283; b) W. R. Wadt, P. J. Hay, *J. Chem. Phys.* **1985**, *82*, 284–298; c) P. J. Hay, W. R. Wadt, *J. Chem. Phys.* **1985**, *82*, 299–310.

Received: December 15, 2012
Published Online: March 6, 2013

 © 2013 Wiley-VCH Verlag GmbH & Co. KGaA, Weinheim